

# Reconstruct hydrological history of terrestrial saline lakes using Mg isotopes in halite: A case study of the Quaternary Dalangtan playa in Qaidam Basin, NW China

Zhiguang Xia<sup>a</sup>, Yongjie Lin<sup>b</sup>, Haizhen Wei<sup>a</sup>, Zhongya Hu<sup>a,c</sup>, Chuan Liu<sup>a</sup>, Weiqiang Li<sup>a,\*</sup>

<sup>a</sup> State Key Laboratory for Mineral Deposits Research, School of Earth Sciences and Engineering, Nanjing University, Nanjing, Jiangsu, China

<sup>b</sup> MNR Key Laboratory of Saline Lake Resources and Environments, Institute of Mineral Resources, Chinese Academy of Geological Sciences, Beijing, China

<sup>c</sup> State Key Laboratory of Marine Geology, School of Ocean and Earth Science, Tongji University, Shanghai, China

## ARTICLE INFO

Editor: A Dickson

### Keywords:

Evaporite  
Paleoclimate  
Qinghai-Tibet plateau  
Xiaoliangshan  
Mg isotopes  
Saline lake  
Halite fluid inclusion

## ABSTRACT

Saline lakes are sensitive to climatic changes, however, it is challenging to reconstruct paleoclimate based on terrestrial evaporite records using conventional elemental and isotopic proxies. Magnesium is a major element in saline lakes, and the Mg isotope composition of brine is responsive to climate-driven processes such as carbonate precipitation and freshwater input. However, little has been explored on the application of Mg isotopes to studies of saline lakes. In this study, the Middle Pleistocene halite deposit from the Xiaoliangshan (XLS) evaporite section in the Qaidam Basin, Northwest China, was selected as a case to evaluate the response of Mg isotopes in the saline lake to environmental events. The Mg isotope data of the halite are complemented by geochemical analyses major elements and Sr-Cl isotopes of the halite component, and C-O isotopes of the associated carbonates. The  $^{87}\text{Sr}/^{86}\text{Sr}$  ratios of the halite remained homogeneous (0.7111 to 0.7112) throughout the section, suggesting that the material source did not change significantly during the precipitation of the halite beds. By contrast, element ratios (Mg/Na and K/Na) and stable isotope ratios of C, O, Cl, and Mg show remarkable fluctuations along with the sediment profile. Based on the C-O-Cl isotope data, we identified events of freshwater recharging and desalination in an overall dry climatic background that were recorded in the halite. Notably, halite  $\delta^{26}\text{Mg}$  values vary by up to 2‰ in the section (from  $-1.63\text{‰}$  to  $0.46\text{‰}$ ), and the low  $\delta^{26}\text{Mg}$  signature of halite was interpreted to reflect the input of light Mg isotopes into the saline lake in a freshwater recharging event, while the high  $\delta^{26}\text{Mg}$  values were produced by the precipitation of carbonate minerals under arid climatic conditions. Collectively, we suggest that Mg isotopes in terrestrial halite could be a sensitive tracer of basin hydrology. This study for the first time demonstrates the potential of Mg isotopes in terrestrial evaporites to unravel paleoclimatic events.

## 1. Introduction

The formation and evolution of saline lakes are complex processes that are closely related to the hydrological, climate, and geological settings of the basin (Babel and Schreiber, 2014; Deocampo and Jones, 2014; Eugster, 1980; Warren, 2016). Climate plays a vital role in producing saline lakes by maintaining a negative water balance in the basin (e.g., Deocampo and Jones, 2014; Hay et al., 2006). Modern and ancient terrestrial evaporites in saline lake basins are unique geological archives for past climates in arid terrains (Babel and Schreiber, 2014; Lowenstein et al., 1999; Warren, 2010). Significant efforts have been made to

constrain paleoclimate information from evaporites using geochemical indicators such as elemental ratios (Br/Cl and K/Cl ratio, Luo et al., 2016; Sun et al., 2019), radiogenic isotopes ( $^{87}\text{Sr}/^{86}\text{Sr}$  ratios, Ullman and Collerson, 1994), and light stable isotopes (such as  $\delta^{11}\text{B}$ ,  $\delta^{13}\text{C}$ ,  $\delta^{18}\text{O}$  and  $\delta^{37}\text{Cl}$ , e.g., Du et al., 2019; Luo et al., 2016; Talbot, 1990). However, conventional tools of the elemental ratio of the bulk sample are susceptible to the variability of fluid inclusion density in evaporites, whereas isotopic tracers of carbonate  $\delta^{13}\text{C}$  and  $\delta^{18}\text{O}$  are controlled by multiple factors such as isotope composition of sources, temperature, and primary productivity (Horita, 2014; Li and Ku, 1997). These limitations induce ambiguity to data interpretation, and new tools are

\* Corresponding author.

E-mail addresses: [991225015@qq.com](mailto:991225015@qq.com) (Z. Xia), [linyongjie2014@163.com](mailto:linyongjie2014@163.com) (Y. Lin), [haizhenwei@nju.edu.cn](mailto:haizhenwei@nju.edu.cn) (H. Wei), [zhongyahu@tongji.edu.cn](mailto:zhongyahu@tongji.edu.cn) (Z. Hu), [609418055@qq.com](mailto:609418055@qq.com) (C. Liu), [liweiqiang@nju.edu.cn](mailto:liweiqiang@nju.edu.cn) (W. Li).

<https://doi.org/10.1016/j.palaeo.2021.110804>

Received 3 September 2021; Received in revised form 8 December 2021; Accepted 15 December 2021

Available online 20 December 2021

0031-0182/© 2021 Elsevier B.V. All rights reserved.

required to overcome the challenges in the paleoclimate reconstruction of evaporite records.

Over the past two decades, advances in multi-collector inductively coupled plasma mass spectrometry (MC-ICP-MS) have enabled high precision isotope analysis for metals such as Mg (Johnson et al., 2004; Teng, 2017). Magnesium is a major element in evaporites and brines, and the Mg isotope composition of brine in the terrestrial basin is controlled by the mass balance of source (river input) and sink (carbonate precipitation) under different hydrological conditions (Shalev et al., 2018a). River waters show large Mg isotope variability (e.g., Tipper et al., 2006; Zhang et al., 2018), and precipitation of carbonate is associated with significant Mg isotope fractionation (e.g., Chen et al., 2020; Immenhauser et al., 2010; Li et al., 2015; Mavromatis et al., 2013; Wang et al., 2013). Thus the  $\delta^{26}\text{Mg}$  value of brine and precipitated halite has the potential to record the history of basin hydrology. However, the applications of Mg isotopes to evaporite and saline lake studies are rare

(Feng et al., 2018; Li et al., 2011; Shalev et al., 2021), especially in halite deposits, the most ubiquitous and abundant evaporite phase. Recently, the successful establishment of a high-precision Mg isotope analytical method for halite provides the possibility for the application of Mg isotopes to the study of evaporites (Xia, 2020; Zhang, 2021).

The Qinghai-Tibet Plateau (QTP) is the most saline lake-rich region in China, where more than 300 saline lakes occur, accounting for over one-third of the surface area of all lakes in the region (Zheng et al., 1993). The Qaidam Basin is a large intermontane basin in the northeast QTP, and one notable fossil saline lake system in the Qaidam Basin is the Dalangtan (DLT) Playa, as its surrounding hyperarid region have been proposed as a potential analog site for Mars surface (e.g., Anglés and Li, 2017; Wang et al., 2010; Xiao et al., 2017; Zheng et al., 2009). The sediments and climatic settings of the DLT playa over the past few decades have been documented (Kong et al., 2018; Sobron et al., 2018). However, few studies focus on the evolution of the hydrological

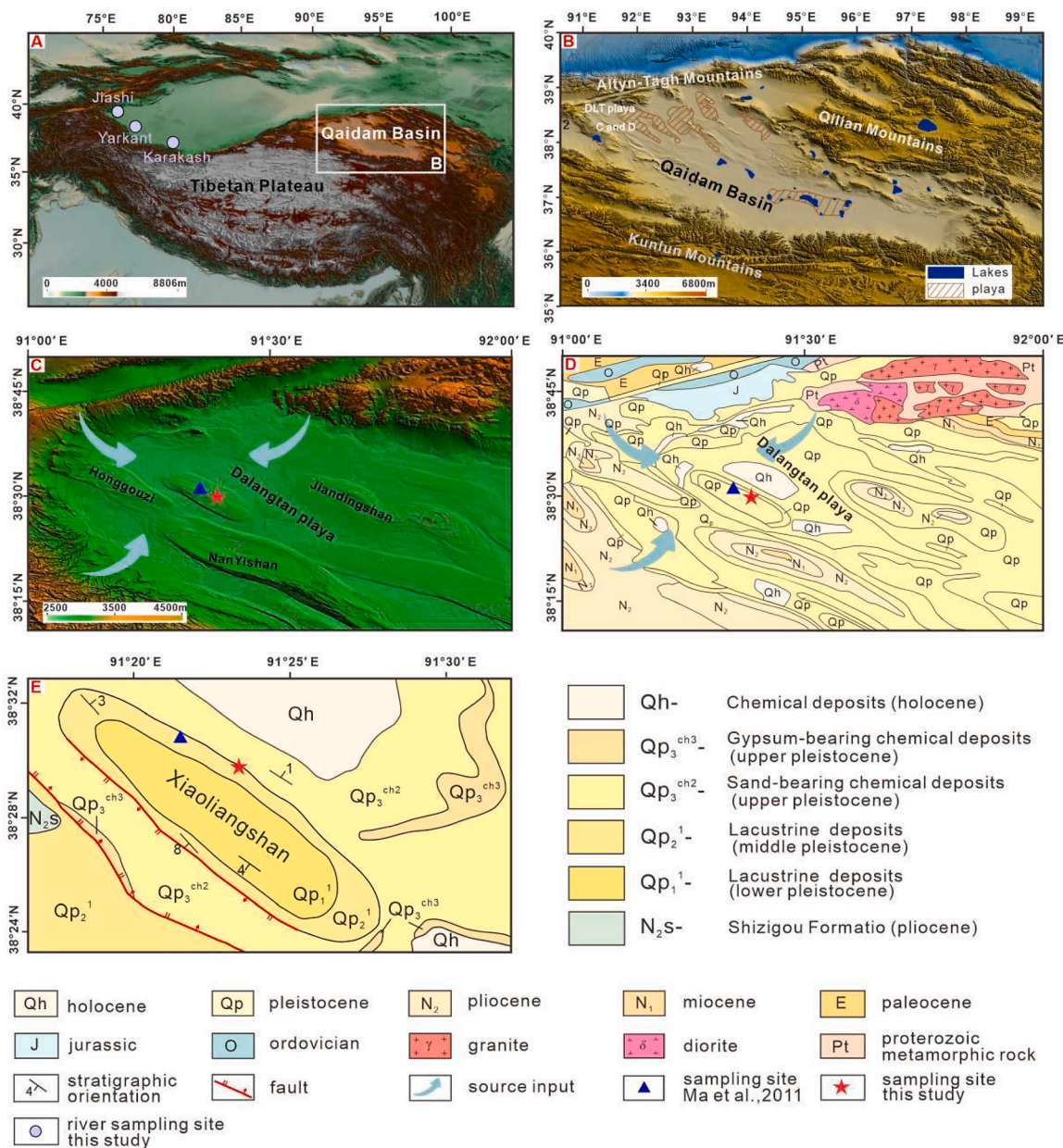


**Fig. 1.** Topographic and geologic maps of the study area. (A)-(C) are the topographic maps of the Qinghai-Tibet Plateau, Qaidam Basin, and Dalangtan area, respectively. Elevation and topography data are derived from <https://srtm.csi.cgiar.org/>. The locations of lakes and playas in Fig. 1B are from Cheng et al. (2021). (D)-(E) Geologic maps of the study area (modified from Kong et al., 2014; Ma et al., 2011).

environment in the DLT playa during the Middle Pleistocene. This study focuses on the primary (unaltered) evaporite samples dominated by halite from the Middle Pleistocene Xiaoliangshan (XLS) section, southwestern DLT playa. We measured Mg isotopes in halite, together with C-O-Cl-Sr isotopes from the same samples, to fingerprint the hydrological fluctuations recorded in Middle Pleistocene halite precipitates. This study shows that  $\delta^{26}\text{Mg}$  value of halite could be a sensitive tracer for drying and recharging events of terrestrial saline lakes.

## 2. Geological setting and samples

The Qaidam Basin, located at the northeastern edge of the QTP, is surrounded by the Kunlun Mountains to the south, Altyn-Tagh Mountains to the west, and Qilian Mountains to the east (Fig. 1). Initiation of the formation of the Qaidam Basin dated back to the Mesozoic (Huang et al., 1993). The current geomorphology of the Qaidam Basin and the distribution of saline lakes are mainly defined by tectonic deformation during the mid-late Pleistocene (e.g., Guo et al., 2018; Huang et al., 1993; Kong et al., 2018). The Qaidam Basin is a hyperarid region due to the blockage of the moist Indian Ocean monsoon by the Himalayas mountain chain (Wang et al., 2018; Wang, 2006). The depositional history of evaporites in the Qaidam Basin is complicated because the sedimentary centers have migrated over time (Huang et al., 1993; Zheng, 1997). In the Qaidam Basin, three major playas of different salt types have been documented: the Mg-sulfate-rich DLT playa, the chloride-rich Qarhan playa, and the sulfate-chloride-rich Kunteyi playa

(e.g., Huang et al., 1993; Kong et al., 2018; Zheng, 1997). The DLT Basin is the deposition center of the west margin Qaidam Basin, with a yearly average temperature of 3.5 °C and annual total precipitation of 50 mm, but annual average evaporation of 2590 mm (Kong et al., 2018). The DLT playa was formed by the drying up of sulfate brine, with mirabilite ( $\text{Na}_2\text{SO}_4 \cdot \text{H}_2\text{O}$ ) and halite being the predominant evaporite minerals in the area (Kong et al., 2018). Due to the arid environment and the presence of salt types that are similar to those found on Mars, this locality has been suggested as a potential Mars analog site (e.g., Anglés and Li, 2017; Wang et al., 2010; Xiao et al., 2017; Zheng et al., 2009).

The XLS anticline was formed during the Middle Pleistocene (Ma et al., 2011). It is located on the southwest side of DLT playa, only a few kilometers from the DLT playa center. The XLS anticline hosts a large amount of Cenozoic sediments, and these strata are distributed along a NW-SE trend. Neogene mudstone, sandstone, marl, limestone, and gypsum strata dominate in the southwest of the XLS area, and Jurassic and Ordovician strata are exposed in the northwest. Proterozoic gneiss, amphibolite, marbles, and early Paleozoic granite and diorite intrusions are exposed in the northeast of the XLS area (Fig. 1).

An outcrop (Lat 38°29'48.60"N, Long 91°23'22"E; Elevation: 2711 m) of a halite-rich interval of the deposit was discovered near the entrance of China Agricultural Potash Fertilizer Factory in the XLS anticline during fieldwork in June 2016. Thin dark clay-rich inter-layers also occur in the halite deposit. The exposed halite beds, about 1.8 m in total thickness, are sandwiched between gypsum deposits above and below and are sub-parallel to the land surface (Fig. 2). The halite

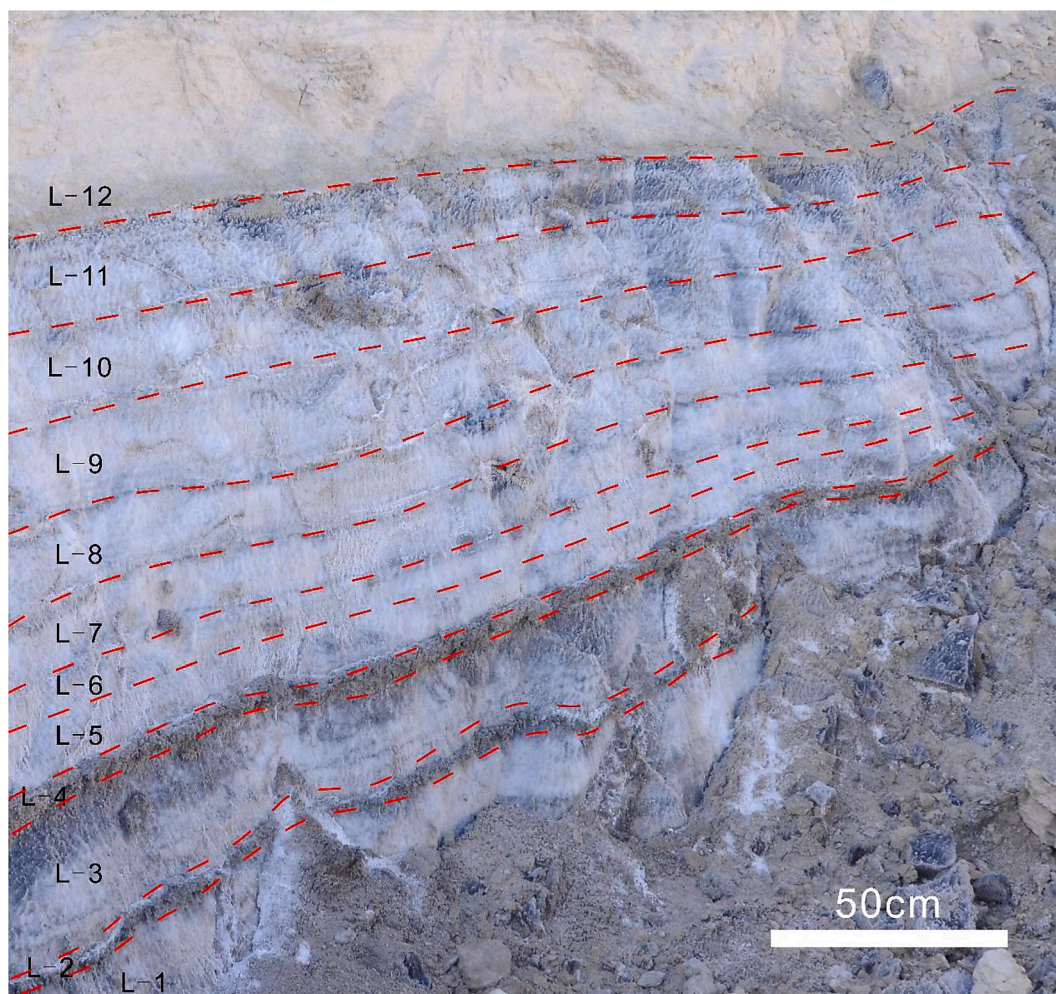


Fig. 2. Field photo of the XLS section. The white halite deposits are intercalated with dark clay-rich layers, and the top and bottom of the halite beds are gypsum deposits.

deposits are exceptionally fresh, showing no evidence of secondary alteration or deformation in the outcrop. After removing the weathered surface crust, twelve pristine halite samples were systematically collected from different horizons that were numbered 1 (bottom) to 12 (top). A large number of liquid phase inclusions were observed in halite crystals under a microscope. The fluid inclusions have diameters ranging from 10 to 50  $\mu\text{m}$  and cluster in chevron-shaped bands of the halite crystals, representing the growth zoning of the halite cube faces (Fig. 3). This indicates that the inclusions are primary inclusions trapped during halite growth in brine during the deposition of halite beds (Roberts and Spencer, 1995).

In addition to the halite beds from the DLT playa, to better characterize the source of the Qaidam Basin, river water samples from three rivers (Jiashi River, Yarkant River, and Karakash River) originated from the Kunlun Mountains were collected for Sr-Mg isotope analysis (Fig. 1).

### 3. Methods and analyses

For laboratory analyses, all salt samples collected from the field were first cleaned by wiping with lint-free paper towels (Kimwipes®) and then sampled with a tungsten carbide scraper to separate fresh, contaminant-free aggregates of salts. The salt aggregates were ultrasonically cleaned in anhydrous ethanol (>99.7%) for 5 min. Then the samples were dried, gently crushed to powders, which were analyzed by XRD for mineral identification. The water-soluble fraction of the sample was subjected to major element and Mg-Cl-Sr isotope analyses. A fraction of the residual water-insoluble components was further analyzed for powder XRD patterns and bulk sample C-O isotope ratios, the rest of water-insoluble residues were treated with acetic acid for major element analysis of acid-leachable components. All analyses were performed on facilities at the State Key Laboratory of Mineral Deposit Research, Nanjing University, China.

#### 3.1. Elemental and mineralogical analyses

Powder X-ray diffraction (XRD) analysis was performed on a Rigaku RAPID II X-ray diffractometer. The instrument was operating at 50 kV and 90 mA on a rotating Mo anode X-ray source. The XRD patterns of powdered samples were collected using a two-dimensional image plate with a 9-min exposure time per analysis. Data processing was performed using Rigaku 2DP and Jade 6.5 software (Li et al., 2019).

Approximately 2–3 g of the pre-cleaned sample was dissolved in 12 mL deionized water (18.2 M $\Omega$  cm) in a 15 mL centrifuge tube. After one day, the tube was centrifuged, then the supernatant (dissolved halite solution) was transferred to a clean centrifuge tube. A small aliquot of the solution was taken and diluted gravimetrically for elemental analysis.

The residue after halite dissolution was further washed with deionized water three times and dried. The solid was then separated into three aliquots, one for C and O isotope analysis of the carbonate fraction (about 1–3 mg is sufficient), one for XRD analysis to determine the mineralogy of water-insoluble components, and the other was dissolved in 1 mol/L acetic acid for elemental analysis.

The elemental concentrations were measured using ICP-OES (for Mg, Ca, Sr, Mn, Fe, and Al) and flame photo spectrometry (for Na and K). A series of gravimetrically prepared commercially-available multi-element standards were used for elemental analysis on both instruments. The calibration curves for the measured elements showed excellent linearity, with linear correlation coefficients ( $R^2$ ) better than 0.999. A multi-element standard solution (1 ppm) was measured before and after each batch of ten samples for monitoring and correction of instrument drift. For assurance of analytical accuracy, standard IAPSO seawater was analyzed as an unknown sample and the measured concentrations of Mg (1233 ppm) and Ca (393 ppm) are consistent with the literature values (Pilson, 2012). The external analytical error of elemental analyses is less than 10% (2RSD, or two times of relative standard deviation).

#### 3.2. Isotopic analyses

##### 3.2.1. Carbon and oxygen isotopes

Carbon and oxygen isotopes were measured using a Thermo Finnigan Delta V Plus continuous flow isotope ratio mass spectrometer (IRMS). Carbonate powder was reacted with orthophosphoric acid for >12 h at 70 °C on a Gas Bench II connected to the IRMS. Both the C and O isotope ratios were reported in standard per mil (‰) notation relative to the Vienna PDB standard. The standard TTB-1 (GBW-04405) was measured during the analytical session and yielded results of  $0.69 \pm 0.12\text{‰}$  for  $\delta^{13}\text{C}$  and  $-8.50 \pm 0.11\text{‰}$  (2SD,  $n = 36$ ) for  $\delta^{18}\text{O}$ , which are consistent literature values (Wang et al., 2021). The long-term external analytical precision was better than  $\pm 0.5\text{‰}$  for both  $\delta^{13}\text{C}$  and  $\delta^{18}\text{O}$  values (Li et al., 2019).

##### 3.2.2. Strontium isotopes ( $^{87}\text{Sr}/^{86}\text{Sr}$ )

Based on the result of elemental analysis, an aliquot of the halite solution or river water containing 500 ng Sr was dried down in a Teflon beaker, converted to nitrate form, and re-dissolved in 0.5 mL 3 N HNO<sub>3</sub> for chemical purification. Strontium was purified following a cation exchange procedure with Sr-spec resin (De Muynck et al., 2009). USGS igneous reference material AGV-2 was processed as unknowns with the samples for quality control. Strontium isotope ratios were measured using a Finnigan Triton thermal ionization mass spectrometer (TIMS).  $^{87}\text{Sr}/^{86}\text{Sr}$  ratios were normalized to  $^{86}\text{Sr}/^{88}\text{Sr} = 0.1194$  using exponential law. The measured  $^{87}\text{Sr}/^{86}\text{Sr}$  ratios of the AGV-2 ( $^{87}\text{Sr}/^{86}\text{Sr}_{\text{AGV-2}} = 0.703966 \pm 6, 1\text{SE}$ ) and NIST 987 ( $^{87}\text{Sr}/^{86}\text{Sr}_{\text{NIST 987}} = 0.710231 \pm 5,$

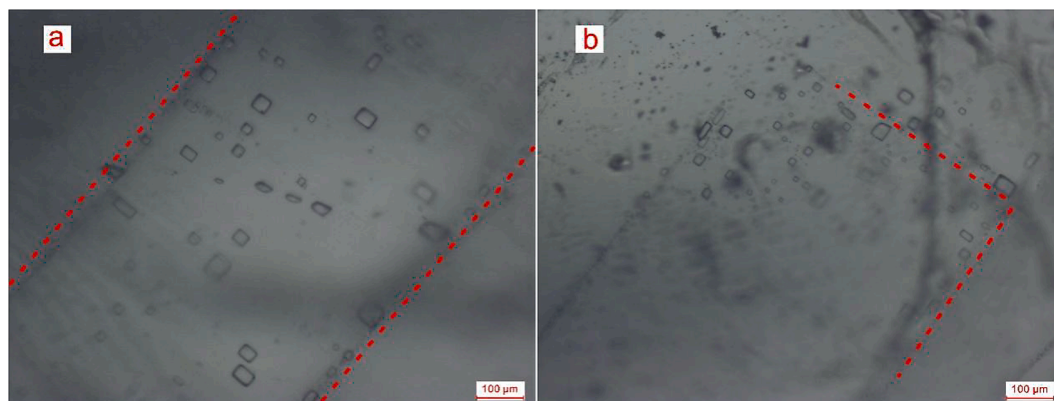


Fig. 3. Photomicrographs showing primary fluid inclusion banding in XLS halite. (a) The liquid-rich fluid inclusions cluster from the L-10 sample are distributed in bands; (b) The liquid-rich fluid inclusions from the L-11 sample developed the chevron structures.

1SE) agree with published values (Bialik et al., 2018; Hu et al., 2017). The long-term external reproducibility (2 standard deviation or 2SD) of NIST 987 yielded  $^{87}\text{Sr}/^{86}\text{Sr} = 0.710228 \pm 0.000034$  ( $2\sigma$ ,  $n = 94$ ).

### 3.2.3. Chlorine isotopes ( $\delta^{37}\text{Cl}$ )

For Cl isotope analysis of dissolved halite, the chlorine in halite solution was converted to CsCl form following an established Cs-Form cation exchange procedure (Wei et al., 2012; Xiao et al., 2002). The isotopic standard reference material ISL354 was processed as unknowns with the samples for column chemistry quality control. Chlorine isotope ratios were measured using a Finnigan Triton thermal ionization mass spectrometer (TIMS). The reference materials ISL354 and NIST 975 ( $\delta^{37}\text{Cl}_{\text{ISL354}} = 0.11 \pm 0.09\%$ ,  $\delta^{37}\text{Cl}_{\text{NIST975}} = 0.37 \pm 0.11\%$ , 2SE,  $n = 2$ ) were used to assess analytical accuracy. All data are reported in  $\delta$  notation as  $\delta^{37}\text{Cl} = [(^{37}\text{Cl}/^{35}\text{Cl}_{\text{sample}})/(^{37}\text{Cl}/^{35}\text{Cl}_{\text{SMOC}}) - 1] \times 1000$  relative to the Chlorine isotope standard SMOC. An aliquot of the ISL354 standard was processed as an unknown sample, and the measured result verified the accuracy of the method ( $\delta^{37}\text{Cl}_{\text{ISL354}} = 0.00 \pm 0.08\%$ , 2SE,  $n = 3$ ). The measured  $\delta^{37}\text{Cl}$  values of these reference materials are consistent with the published values (Xiao et al., 2002). The external precision of measured  $\delta^{37}\text{Cl}$  is better than  $\pm 0.3\%$  (2SE, two standard error).

### 3.2.4. Magnesium isotopes ( $\delta^{26}\text{Mg}$ )

Halite samples contain a large amount of Na and Ca as the matrix elements. A technique of pre-enrichment of Mg by  $\text{Mg}(\text{OH})_2$  precipitation (Xia et al., 2020) was applied to separate the majority of Na from Mg. After the pre-enrichment, the Na: Mg ratio of the halite sample was significantly reduced. Then the Mg was purified following a two-stage ion exchange procedure that has been described in Hu et al. (2017). Magnesium isotope ratios were measured using a Thermo Scientific NEPTUNE Plus multi-collector MC-ICP-MS. Instrumental drift and mass bias were corrected by the standard-sample-standard bracketing method, with concentrations of both standard and sample solutions prepared to be within  $1 \pm 0.1$  ppm. A pure Mg stock solution (HPS909104) from High Purity Standards Inc. ( $\delta^{26}\text{Mg}_{\text{HPS909104}} = -0.65 \pm 0.03\%$ , 2SD,  $n = 4$ ) was used as an in-house bracketing Mg standard (Li et al., 2015; Li et al., 2012a). The international Mg isotope standards DSM3 and Cambridge1 were measured, which verified the analytical accuracy of mass spectrometry ( $\delta^{26}\text{Mg}_{\text{DSM3}} = -0.02 \pm 0.10\%$ ,  $\delta^{26}\text{Mg}_{\text{Cambridge1}} = -2.62 \pm 0.02\%$ , 2SD,  $n = 8$ ). Additionally, USGS igneous rock standard (DTS-2) and IAPSO seawater were treated as unknown samples to verify the accuracy of chemical procedures ( $\delta^{26}\text{Mg}_{\text{DTS-2}} = -0.25 \pm 0.06\%$ ,  $\delta^{26}\text{Mg}_{\text{IAPSO Seawater}} = -0.83 \pm 0.01\%$ , 2SD,  $n = 4$ ). All data are reported in  $\delta$  notation as  $\delta^{26,25}\text{Mg} = [(^{26,25}\text{Mg}/^{24}\text{Mg}_{\text{sample}})/(^{26,25}\text{Mg}/^{24}\text{Mg}_{\text{DSM3}}) - 1] \times 1000$  relative to the international Mg isotope standard DSM3. Based on repeated analysis of multiple geological standards and Mg standard solutions, the long-term external reproducibility of  $\delta^{26}\text{Mg}$  is better than  $\pm 0.1\%$ .

## 4. Results

### 4.1. Major elements and mineralogy

The chemical compositions of the water-soluble components of the evaporite samples are shown in Table 1. Besides the very high Na content that is consistent with the predominance of halite in the evaporite samples, most of the samples have remarkably high calcium contents, which may reflect the partial dissolution of gypsum in the samples. Samples L-3 and L-12 have the highest Mg (1936 ppm) and K contents (333 ppm). Bulk sample XRD results show that the samples L-3 and L-12 are mainly composed of halite and quartz, with minor gypsum and carbonate minerals. XRD-detectable minerals of other samples are only halite and quartz (Fig. 4a). No water-soluble Mg-K evaporite minerals (i. e., epsomite or polyhalite) were detected by XRD in all analyzed samples. In addition, the XRD results show that the water-insoluble

**Table 1**  
Elemental concentration and isotopic composition of XLS halite and the river originating from the Kunlun Mountains.

Sample number	depth (cm)	weight(g)	water-insoluble weight(g)	Na( $\times 10^3$ ppm)	Mg(ppm)	K(ppm)	Ca(ppm)	Sr(ppm)	$^{87}\text{Sr}/^{86}\text{Sr}$	1SE	$\delta^{26}\text{Mg}^f$	2SD	$\delta^{26}\text{Mg}^p$	2SD	$\delta^{37}\text{Cl}$	2SE
L-12	5	2.545	1.686	72.0	147	241	1007	6.5	0.711142	5.8E-06	-0.42	0.02	-0.49	0.04		
L-11	20	2.621	0.015	88.6	16	12	123	1.0	0.711238	4.9E-06	-0.84	0.06	-1.06	0.00	0.31	0.24
L-10	35	2.879	0.056	91.2	22	18	555	2.5	0.711151	5.4E-06	-1.09	0.02	-0.93	0.04	0.14	0.26
L-9	53	2.967	0.023	95.0	21	19	229	3.5	0.711163	4.9E-06	-0.68	0.07	-0.72	0.09	0.57	0.14
L-8	73	2.796	0.065	91.0	28	20	206	3.3	0.711165	4.9E-06	-0.65	0.05	-0.58	0.02	0.50	0.22
L-7	88	2.876	0.001	94.0	17	16	188	3.8	0.711167	4.7E-06	-0.51	0.01	-0.51	0.03	0.26	0.19
L-6	98	2.892	0.001	93.0	8	11	4	1.8	0.711143	5.7E-06	-0.44	0.05	-0.29	0.01	0.60	0.05
L-5	118	2.886	0.001	94.0	14	13	6	0.4	0.711135	5.1E-06	-0.40	0.02	-0.33	0.07	0.11	0.30
L-4	119	2.257	-	48.8	59	17	120	2.6	0.711124	4.2E-06	-1.63	0.05	-1.99	0.02	-0.10	0.29
L-3	149	3.138	1.407	59.4	1936	334	1073	20.0	0.711121	4.5E-06	0.42	0.02	0.05	0.07		
L-2	152	2.785	0.237	86.0	76	32	591	18.5	0.711118	5.3E-06	0.14	0.02	0.06	0.01		
L-1	172	2.892	0.006	94.0	25	10	22	0.4	0.711110	4.4E-06	0.24	0.10	0.11	0.03	0.17	0.28
Jiashi river																
Yarkant River-edge																
Yarkant River-center																
Karakash River-upstream																
Karakash River-downstream																

Note: The ‘f’ and ‘p’ represent the first batch of analyses for halite in April 2019 and the duplicate analyses on different parts of halite samples in September 2019, respectively.

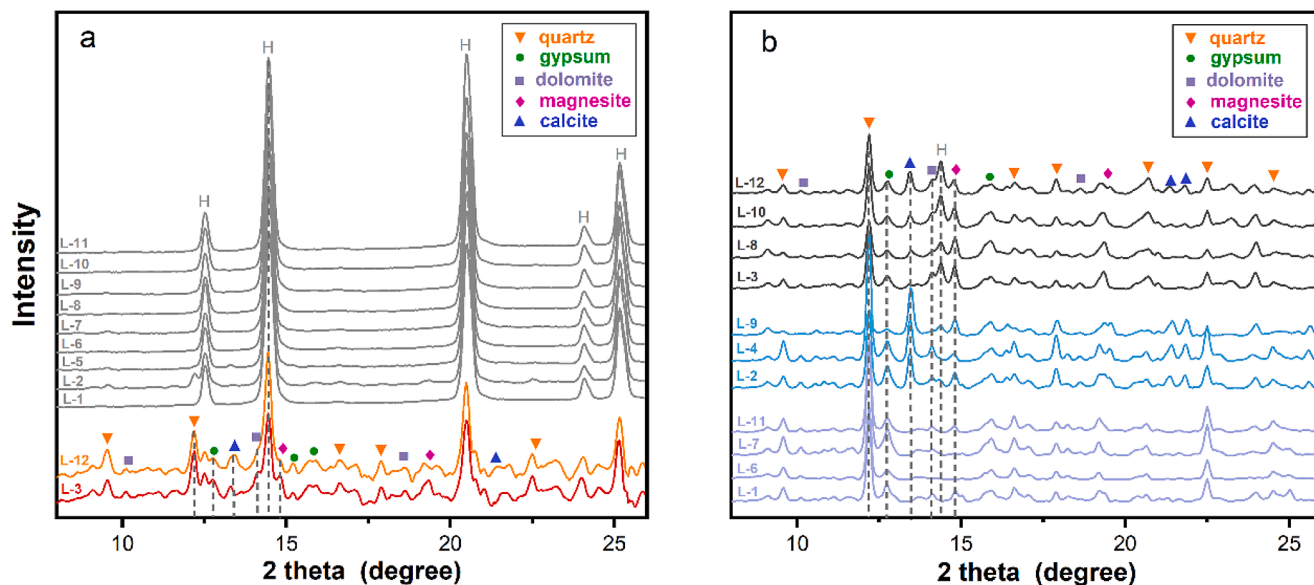


Fig. 4. XRD spectra of the bulk sample (a) and the water-insoluble fraction (b) of the halite samples, “H” denotes halite. The samples are dominated by halite, followed by quartz, gypsum and carbonate minerals such as dolomite, magnesite, and calcite.

materials are composed of quartz, carbonate minerals, and a small amount of gypsum. Trace amounts of halite peaks in the XRD spectrum reflected incomplete water-leaching of the halite samples (Fig. 4b).

Results of elemental analysis of the acetic acid leachates are shown in Table 2. The high contents of Mg (3.0–11.7 wt%) and Ca (0.7–15.1 wt%) in the acid-leachable fraction of the solid are expected, and the moderate concentrations of Al (51–8446 ppm) are indicative of leaching of silicious components such as clays. The measured Ca and Mg contents suggest the existence of Mg-bearing carbonate minerals (e.g., magnesite and dolomite) in the acid-leachable fractions. In addition, the samples have high Sr and low Mn contents, with Mn/Sr ratios of below 2, a threshold value for significant carbonate diagenesis in marine carbonate deposits. The ternary diagram based on the results of major elements shows that  $MgCO_3$  and  $CaCO_3$  are the prominent components of the carbonates (Fig. 5), consistent with the XRD observation that the main carbonate minerals are magnesite and dolomite.

#### 4.2. Isotopic compositions

$^{87}Sr/^{86}Sr$  ratios of the halite samples range between  $0.711110 \pm 4$  and  $0.711238 \pm 5$  (1SE), averaging at  $0.711148$  ( $n = 12$ ). The variability in  $^{87}Sr/^{86}Sr$  ratios of the samples is comparable to the external uncertainty of the analytical method. Thus, there is no apparent stratigraphic variation trend of  $^{87}Sr/^{86}Sr$  ratios (Figs. 6 and 9). For comparison, the  $^{87}Sr/^{86}Sr$  ratios of the three rivers originating from the Kunlun Mountains range from 0.7088 to 0.7124, with an average value of 0.7111 (Table 1).

Carbonates in the evaporite samples from the XLS section have  $\delta^{13}C_V$ .

Table 2  
Elemental concentration and isotopic composition of carbonates component.

Sample number	Mg( $\times 10^3$ ppm)	Ca( $\times 10^3$ ppm)	Fe( $\times 10^3$ ppm)	Al-ppm	Sr-ppm	Mn-ppm	$\delta^{13}C$	$\delta^{16}O$	$\delta^{26}Mg$	2SD
L-12-HAC	42.5	91.5	2.5	137	928	198	2.18	7.48	-2.04	0.09
L-11-HAC	117.7	107.3	17.5	5221	659	950	1.58	8.02	-1.98	0.03
L-10-HAC	81.0	52.8	4.5	663	942	419	1.78	9.98	-1.86	0.07
L-9-HAC	216.6	151.1	22.4	4546	1623	1178	1.93	6.63	-1.98	0.02
L-8-HAC	79.6	7.5	0.8	132	194	66	1.38	6.78	-1.24	0.00
L-7-HAC	34.1	26.5	23.1	8446	263	479	1.28	-0.87	-0.70	
L-4-HAC							1.32	-0.70		
L-3-HAC	29.8	76.8	3.2	51	793	135	2.34	9.93	-1.48	0.03
L-2-HAC	50.5	43.8	2.5	364	896	277	1.69	3.36	-1.68	0.06
L-1-HAC	58.4	17.8	14.6	4718	510	408	1.41	-1.03	-1.60	0.03

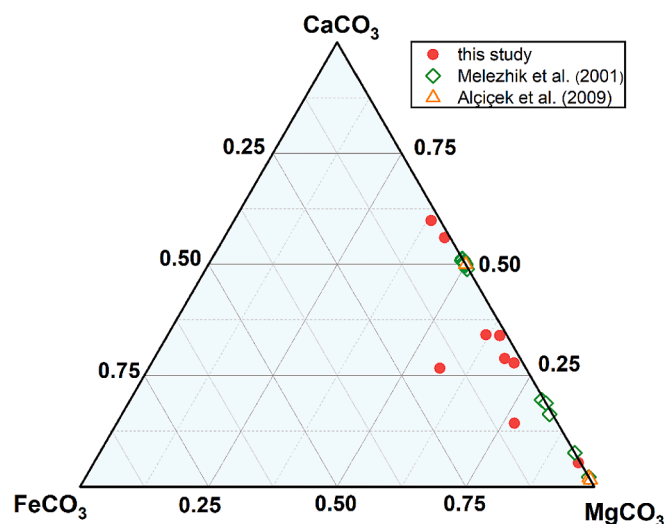
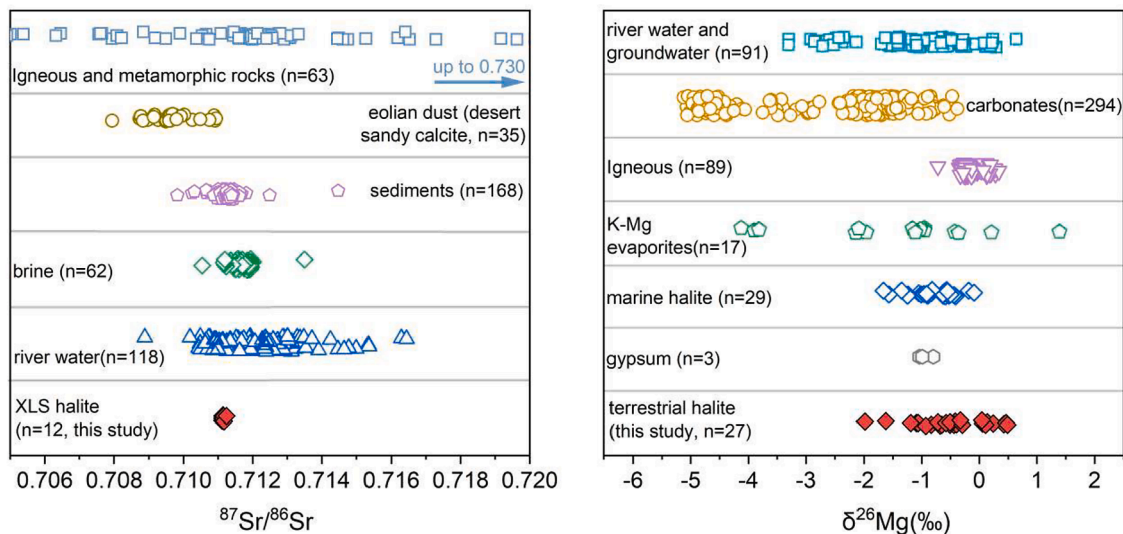


Fig. 5. Ternary diagram of carbonate composition (molar fractions) for the water-insoluble fraction of halite samples from XLS section (filled red circles), with comparison of data from literature (Alçiçek, 2009; Melezhik et al., 2001). (For interpretation of the references to colour in this figure legend, the reader is referred to the web version of this article.)



**Fig. 6.** Sr-Mg isotope data for the XLS halite samples (red diamonds), with a comparison to published Sr isotope data for different reservoirs from the Tibetan plateau, and published Mg isotope data for different reservoirs from world-wide samples. The list of source literature for the published Sr and Mg isotope data is provided in online appendix B. (For interpretation of the references to colour in this figure legend, the reader is referred to the web version of this article.)

PDB values of 1.28‰ to 2.34‰ and  $\delta^{18}\text{O}_{\text{V-PDB}}$  values of  $-0.87\text{‰}$  to 9.98‰ (Table 2). The  $\delta^{37}\text{Cl}$  values in the halite of the XLS section range from  $-0.1\text{‰}$  to 0.6‰, with sample L-3 having the lowest  $\delta^{37}\text{Cl}$  value (Table 1).

The  $\delta^{26}\text{Mg}$  values of halite show a considerable variation ( $-1.63\text{‰}$  to 0.46‰), while the  $\delta^{26}\text{Mg}$  values of the three rivers show a limited range ( $-1.51\text{‰}$  to  $-1.13\text{‰}$ ) (Table 1). Complete duplicate analyses of different parts of the rock salt were performed in two different analytical campaigns that were six months apart, in which different halite dissolution time was used (i.e., one day and ten days), yet  $\delta^{26}\text{Mg}$  values obtained from the two sessions are consistent (Fig. 8), attesting to the accuracy and reproducibility of the analytical method.

## 5. Discussion

The chemical and isotopic variability in lacustrine sediments could be caused by changes in the sources and changes in the environmental conditions, therefore it is necessary to separate the influence of the two factors. In this section, we first evaluate the potential variability in sources for the deposits in the XLS section by halite  $^{87}\text{Sr}/^{86}\text{Sr}$  ratios, then we concentrate on major elements and stable isotope signatures of the halite and associated carbonates for paleo-climate indications. Finally, the response of halite Mg isotopes to basin hydrology is discussed.

### 5.1. Basin provenance constrained from $^{87}\text{Sr}/^{86}\text{Sr}$ ratios

The DLT Basin was the sedimentary center of the west Qaidam Basin during the Pleistocene (Huang et al., 1993; Zheng, 1997), thus weathering of the surrounding sedimentary rocks (Neogene, Jurassic, and Ordovician strata), magmatic rocks (granite and diorite) and metamorphic rocks (gneiss) contributed source materials to the basin. The Sr isotope signatures of the brine in the saline lakes can be preserved in the evaporite records (Flecker et al., 2002; Lu and Meyers, 2003). Fan et al. (2018) reported a large variation in  $^{87}\text{Sr}/^{86}\text{Sr}$  of the river water, brine, hot spring water, and halite in the Qaidam Basin, illustrating the usefulness of  $^{87}\text{Sr}/^{86}\text{Sr}$  in provenance study for saline lakes. The Sr isotopic compositions of different sources in the eastern and northern QTP, including igneous and metamorphic rocks, sediments, eolian dust, brine, and rivers are compiled (Fig. 6). The  $^{87}\text{Sr}/^{86}\text{Sr}$  ratios of these samples vary from 0.7049 to 0.7302 ( $n = 458$ ), and a large proportion of them are between 0.7100 and 0.7120 (325/458), covering the  $^{87}\text{Sr}/^{86}\text{Sr}$  ratios of the XLS halite samples (from 0.7111 to 0.7112).

The invariant Sr isotopic compositions of XLS halite samples are most parsimoniously explained by the uniformity of the relative contributions of the various sources to the DLT saline lake during the XLS halite precipitation. A similar phenomenon of decoupling of variabilities in paleolake salinity and  $^{87}\text{Sr}/^{86}\text{Sr}$  ratios has also been reported based on a study of Miocene carbonate sediments in the eastern Qaidam Basin (Song et al., 2020). Second, considering the critical role of carbonates and/or evaporites weathering on the riverine Sr flux (Jin et al., 2010; Song et al., 2020; Wu et al., 2009), even if the proportion of silicate weathering versus carbonate weathering had varied slightly (but still dominated by carbonate/evaporites), the  $^{87}\text{Sr}/^{86}\text{Sr}$  ratios of basin brines may not change significantly. In a study of the hydrochemical characteristics of several inland rivers in the northeastern QTP, Wu (2016) provided evidence that silicate weathering in this region is relatively weak. Therefore, the limited variation in  $^{87}\text{Sr}/^{86}\text{Sr}$  ratios of the XLS section indicates that either the provenance of source materials for the basin has not changed during the precipitation of the halite beds, or the Sr input was dominated by carbonate weathering in the source rocks. Both explanations suggest a limited role of source as the cause of the remarkable variations in other geochemical indicators in the halite beds. Thus, the geochemical variabilities in the XLS section are attributed to the hydrological changes during the precipitation of the halite beds.

### 5.2. Constraints of basin hydrological history from conventional elemental and isotopic proxies

#### 5.2.1. The element ratios in halite and their limitations

For typical brine evolution series, in the long interval before the precipitation of Mg-K evaporite minerals (Bäbel and Schreiber, 2014), the behavior of Mg and K elements in brine is conservative, so the content of Mg-K in brine and precipitated halite will increase with evaporation (Bäbel and Schreiber, 2014). Therefore, the K/Cl and Mg/Cl ratios of halite have been used as an indicator for the evolutionary stage of evaporites (Luo et al., 2016), and similarly, the ratios of K/Na and Mg/Na can also be used to qualitatively mark the evaporation stage due to the 1:1 stoichiometry of Na and Cl in halite. Elemental analysis showed that halite sample L-3 has very high Mg/Na and K/Na ratios, which may imply that L-3 was formed in extremely concentrated brines. However, it should be noted that  $\text{K}^+$  and  $\text{Mg}^{2+}$  are present in halite as fluid inclusions (McCaffrey et al., 1987; Moretto, 1988). Therefore, the increase in density of inclusions captured during halite formation could also contribute to the increase in elemental ratios of K/Na and Mg/Na,

thus there is ambiguity in these elemental ratios alone, and additional proxies are needed to provide more substantial constraints on the paleo-hydrological history of saline lakes.

### 5.2.2. Variations in basin hydrology: evidence from C-O-Cl isotopes

The covariance between  $\delta^{13}\text{C}$  and  $\delta^{18}\text{O}$  of lacustrine carbonates can be used to constrain the hydrological history of a basin (Li and Ku, 1997; Talbot, 1990). A positive correlation of carbonate  $\delta^{13}\text{C}$ - $\delta^{18}\text{O}$  values is expected in closed lakes (Talbot, 1990). However, different lakes may exhibit different evolutionary trends in the crossplot of  $\delta^{13}\text{C}$  vs.  $\delta^{18}\text{O}$  due to the differences in the ecological environment, climate, and topography (Benson et al., 2011; Newell et al., 2017) (Fig. 7). For closed-basin lakes, freshwater input generally reduces the  $\delta^{13}\text{C}$  and  $\delta^{18}\text{O}$  values, whereas evaporation leads to increases in  $\delta^{13}\text{C}$  and  $\delta^{18}\text{O}$  values (Li and Ku, 1997). In addition, the  $\delta^{13}\text{C}$  values of carbonates also increase with increasing primary productivity (Li and Ku, 1997; Stiller and Shasha, 1985; Yadav, 1997). The  $\delta^{13}\text{C}$  and  $\delta^{18}\text{O}$  values of the XLS samples exhibit variability and correlation coefficients similar to those of the thenardite-carbonate section reported by Ma et al. (2011). The covariation ( $r = 0.72$ ,  $p < 0.05$ ,  $n = 10$ ) between  $\delta^{13}\text{C}$  and  $\delta^{18}\text{O}$  values suggests closed basin hydrology during halite precipitation. Compared to the steeper slope observed from microbialite samples from the Great Salt Lake, the smaller slope of the data trend for XLS carbonates in the plot of  $\delta^{13}\text{C}$  vs.  $\delta^{18}\text{O}$  implies lower primary productivity (Fig. 7). It is important to note that the  $\delta^{13}\text{C}$  and  $\delta^{18}\text{O}$  values fluctuated along with the depositional profile, reflecting alternating events of freshwater recharge and droughts during the deposition of the halite beds.

Chlorine is abundant in brines and evaporites, and Cl isotope ratios of halite can be used as an alternative approach to constrain the origin and sedimentary stage of the evaporites (e.g., Eastoe and Peryt, 1999; Tan et al., 2006; Tan et al., 2005; Zhao et al., 2020). Specifically, Cl isotopes can be used to distinguish the evolutionary stages of evaporites due to Cl isotope fractionation associated with halite precipitation (e.g., Tan et al., 2006; Tan et al., 2005).  $^{37}\text{Cl}$  is preferentially removed from the brine by halite precipitation, resulting in lower  $\delta^{37}\text{Cl}$  values of the residual brine (Eggenkamp et al., 1995; Luo et al., 2012). Eggenkamp et al. (1995) have suggested that progressive evaporation of brine results in Rayleigh-type Cl isotopic evolution of the halite precipitates and brine in a closed system. Notably, the stratigraphic variations in  $\delta^{37}\text{Cl}$  values of halite in the Zechstein deposits are in general agreement with the

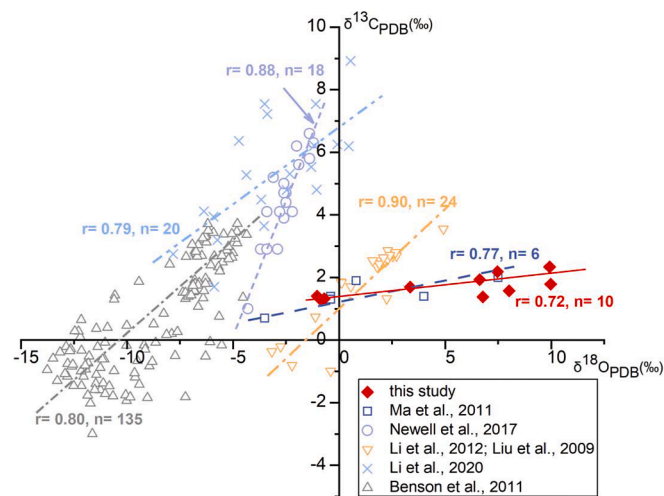


Fig. 7. Cross plot of  $\delta^{13}\text{C}$  versus  $\delta^{18}\text{O}$  for carbonates from the XLS halite samples and samples from other saline lakes, including the Qinghai Lake (Li et al., 2012b; Liu et al., 2009), lakes from other Tibetan Plateau (Li et al., 2020), the Great Salt Lake of the United States (Benson et al., 2011; Newell et al., 2017), as well as a published XLS thenardite-carbonate profile (Ma et al., 2011).

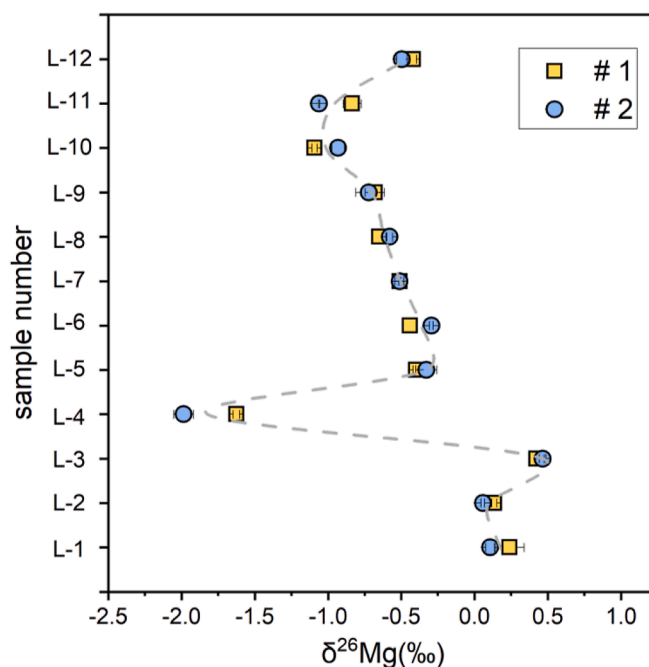


Fig. 8. Stratigraphic variation of the Mg isotope compositions of halite from the XLS section. Data set “#1” represents the first batch of analysis for the halite that was performed in April 2019; data set “#2” are duplicate analyses (independent dissolution and chemical purification) of different aliquots of the halite samples in September 2019.

Rayleigh fractionation model. Thus, the decreasing  $\delta^{37}\text{Cl}$  values in a continuous halite section reflect continuous halite precipitation from brine in a dry environment. By contrast, meteoric river inflow under wetter conditions would cause dissolution of the halite from the previous drought cycles, providing a high  $\delta^{37}\text{Cl}$  source for the basin (Luo et al., 2016). Therefore, the fluctuations in  $\delta^{37}\text{Cl}$  values along with the profile also indicate cycles of evaporation and desalination (Fig. 9).

It should be noted, however, that the trends in  $\delta^{13}\text{C}$ - $\delta^{18}\text{O}$  values of carbonates and  $\delta^{37}\text{Cl}$  values of halite do not correlate perfectly, reflecting mixed influences of temperature and/or primary productivity to the different proxies. Specifically,  $\delta^{13}\text{C}$  values of carbonate can be affected by the primary productivity of the basin (Li and Ku, 1997), whereas  $\delta^{18}\text{O}$  value of carbonate is affected by the brine temperature (Horita, 2014; Xia et al., 1997), yet the observed variation of  $\delta^{37}\text{Cl}$  values are limited due to the small fractionation associated with halite precipitation (Eggenkamp et al., 1995). Nevertheless, the C-O-Cl dataset from the XLS section collectively illustrates that the Dalangtan playa had experienced events of drying as recorded in sample L-3 ( $\delta^{13}\text{C}$  and  $\delta^{18}\text{O}$  values increase,  $\delta^{37}\text{Cl}$  value decrease) and freshwater recharging as recorded in sample L-4 ( $\delta^{13}\text{C}$  and  $\delta^{18}\text{O}$  values decrease,  $\delta^{37}\text{Cl}$  value increase), although the corresponding hydrological conditions of other samples are relatively less clear.

### 5.3. Response of Mg isotopes in halite to hydrological changes in saline lakes

The geochemical behavior of Mg isotopes in different geological processes has been extensively studied over the past two decades (Teng, 2017). However, Mg isotope data from terrestrial evaporite deposits are still scarce, and Mg isotope behavior in saline lake systems remains to be explored. Our work begins to fill this knowledge gap, and the results show significant variability ( $-1.63\text{‰}$  to  $0.46\text{‰}$ ) in  $\delta^{26}\text{Mg}$  values of terrestrial halite deposits (Fig. 6).

The mineralogy of the XLS section is dominated by halite and gypsum, with minor carbonate minerals and clay minerals. This suggests

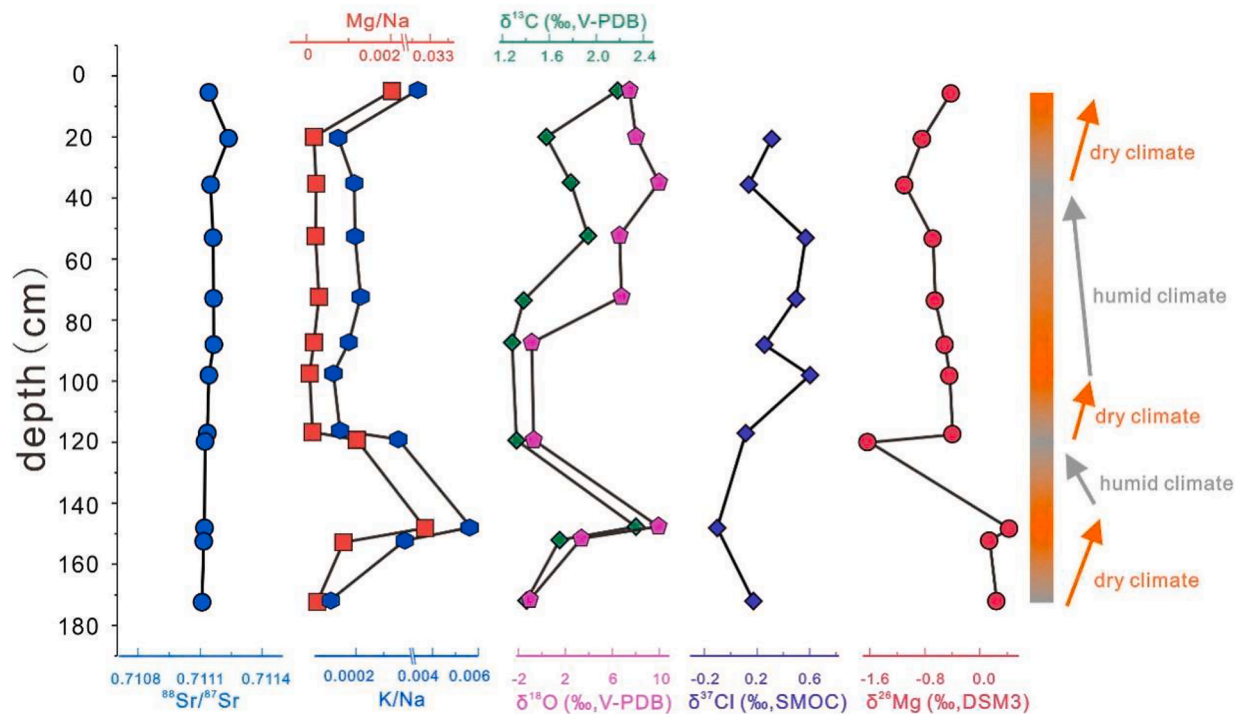


Fig. 9. Stratigraphic variations of elemental (Mg/Na and K/Na) and isotopic (C-O-Cl-Sr-Mg) ratios for the halite bed samples in the XLS section and the inferred hydrological history.

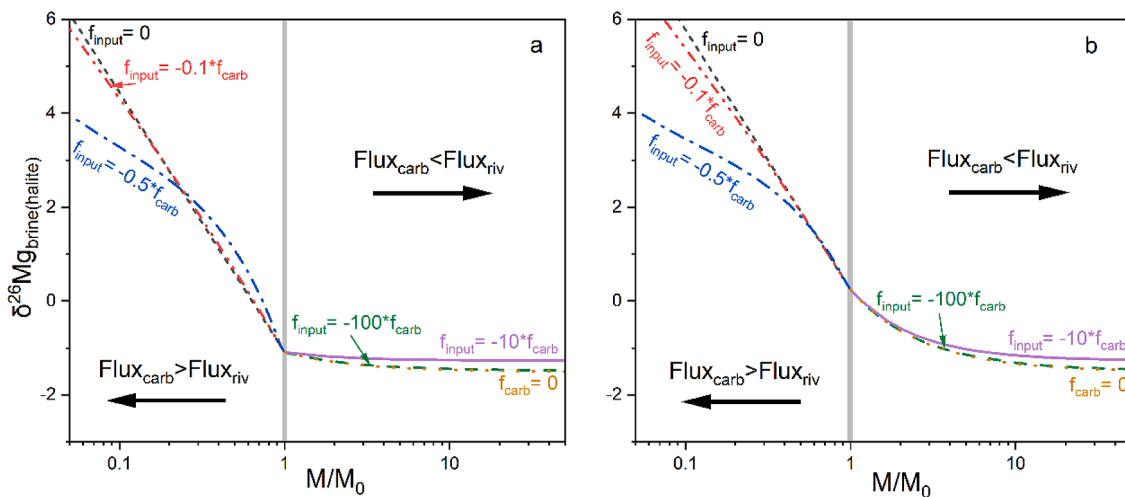
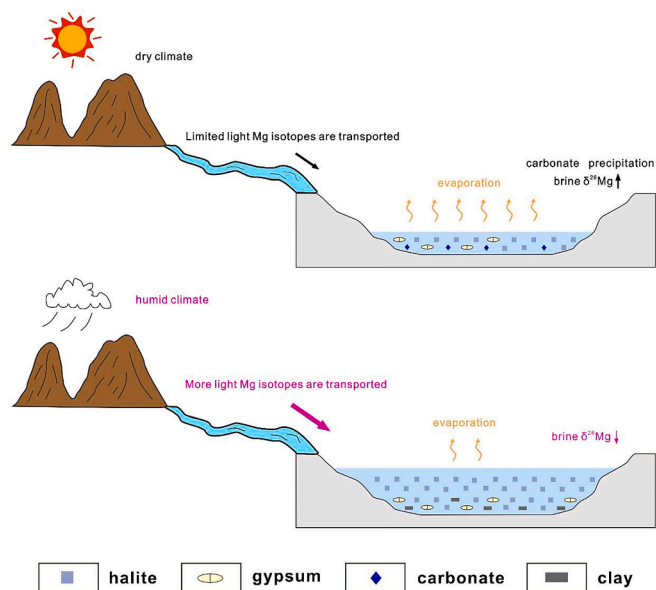


Fig. 10. Modeling results that show the influence of carbonate precipitation and riverine Mg input on the Mg isotope composition of the brine in the saline lake (which will also be trapped in halite fluid inclusions).  $M$  represents the total mass of Mg in the saline lake system at different modeling time ( $M_0$  represent the mass of Mg at the starting time). The  $\delta^{26}\text{Mg}$  values of the initial brine are set to  $-1.09\text{‰}$  and  $0.24\text{‰}$  for plots a and b, respectively. For details, see text.

that the brine was in the early stage and did not reach the stage of Mg-evaporite mineral (such as epsomite or kainite) precipitation (Bäbel and Schreiber, 2014; McCaffrey et al., 1987; Shalev et al., 2018b). No Mg-evaporite minerals were reported in the field investigation of the contemporary mirabilite-carbonate clay interbed profile near the study area (Ma et al., 2011), nor in this study by detailed XRD analyses. Thus, the influence of water-soluble Mg-evaporite minerals on the Mg isotopes of halite should be limited. It is worth noting that the XRD patterns of L-3 and L-12 samples reveal the presence of dolomite and magnesite. The existence of magnesite in the XLS profile is consistent with the experimental study of Hobbs and Xu (2020), who suggested that the lagoon/playa lake environment is favorable for the formation of magnesite. The precipitation of carbonates would change the Mg isotope composition of

the residual brine and the subsequently precipitated halite.

Experimental calibration, theoretical calculations, and observation of natural samples all consistently show that the precipitation of carbonate minerals preferentially removes  $^{24}\text{Mg}$  (e.g., Chen et al., 2020; Immenhauser et al., 2010; Li et al., 2015; Li et al., 2012a; Mavromatis et al., 2013; Pogge von Strandmann et al., 2019; Shalev et al., 2020; Son et al., 2020; Wang et al., 2019; Wang et al., 2013), resulting in enrichment of heavy Mg isotopes in the residual solution. On the other hand, river waters generally have low  $\delta^{26}\text{Mg}$  values ( $-2.52\text{‰}$  to  $+0.64\text{‰}$ , averaging at  $-1.09\text{‰}$ ), particularly for those draining limestone-rich catchment ( $-2.5\text{‰}$ ) (Teng, 2017; Tipper et al., 2006). Considering the occurrence of carbonate strata in the region and the existence of carbonate precipitates in the XLS halite beds, we propose that the



**Fig. 11.** The schematic cartoon illustrating how  $\delta^{26}\text{Mg}$  values of saline lake brine (trapped in halite fluid inclusions) respond to climate and hydrology changes at XLS during the Middle Pleistocene.

significant Mg isotope variation observed in halite samples reflect the balance between river water recharge that brings low  $\delta^{26}\text{Mg}$  to the saline lake, and the precipitation of carbonates, which increases the  $\delta^{26}\text{Mg}$  value of the brine. A conceptual model is constructed to quantitatively evaluate the effects of hydrological changes on the basin brines  $\delta^{26}\text{Mg}$  values. This model considers the isotopic effects of progressive carbonate precipitation that removes light Mg isotopes from the brine following a Rayleigh trend, and riverine input of low  $\delta^{26}\text{Mg}$  Mg into the saline lake that follows a binary mixing relation. The equations that describe the model are:

$$\delta^{26}\text{Mg}_{\text{brine}(c)} = (1000 + \delta^{26}\text{Mg}_{\text{brine}}) \times f^{(\alpha_{\text{carb-sol}} - 1)} - 1000 \quad (1)$$

$$\delta^{26}\text{Mg}_{\text{brine}(r)} = X_{\text{river}} \times \delta^{26}\text{Mg}_{\text{river}} + X_{\text{brine}} \delta^{26}\text{Mg}_{\text{brine}} \quad (2)$$

$\delta^{26}\text{Mg}_{\text{brine}(c)}$  and  $\delta^{26}\text{Mg}_{\text{brine}(r)}$  denote the  $\delta^{26}\text{Mg}$  values of basin brine modified by carbonate precipitates and river water input.  $f$  is the fraction of Mg remaining in brine,  $\alpha_{\text{carb-sol}}$  represents the overall Mg isotope fractionation factor accounting for carbonate precipitation. Considering that the carbonate minerals associated with XLS halite include dolomite ( $\Delta^{26}\text{Mg}_{\text{dolo-solu}} = -1.8\text{‰}$ ,  $T = 20\text{ °C}$ , Li et al. (2015)) and magnesite ( $\Delta^{26}\text{Mg}_{\text{mag-solu}} = -2.8\text{‰}$ , Wang et al. (2019)), an intermediate Mg isotope fractionation factor between the bulk carbonate and aqueous solution is used ( $-2.4\text{‰}$ , correspondence  $\alpha_{\text{bulk carb-sol}} = 0.9976$ ).  $X_{\text{river}}$  and  $X_{\text{brine}}$  represent the proportion of river water Mg flux and initial brine Mg flux in mixed brine, respectively. Since the Pleistocene river water sample is not available in the XLS area at present, the  $\delta^{26}\text{Mg}$  value ( $-1.51\text{‰}$ ) of Jiashi river originating in the Kunlun Mountains was set as the  $\delta^{26}\text{Mg}_{\text{river}}$ . The initial Mg isotope values of the brine were set to  $-1.09\text{‰}$  and  $0.24\text{‰}$  to account for different starting conditions. The former represents the flux-weighted average of global riverine runoff, while the latter represents the  $\delta^{26}\text{Mg}$  brine value during the precipitation of the L-1 samples.  $M_0$  represents the initial Mg fluxes of the basin, and  $M$  represents the Mg flux of modified brine after carbonate precipitation and river Mg input (Fig. 10).

The modeling results show that the Mg isotope composition of the brines is primarily controlled by the relative contribution of different Mg fluxes (Fig. 10 and appendix A). When the Mg flux removed by carbonate precipitation is greater than that of riverine input, the basin brine would gradually enrich  $^{26}\text{Mg}$ . On the contrary, the  $\delta^{26}\text{Mg}$  value of basin

brine would decrease progressively if the influx of isotopically light riverine Mg is greater than the outflux of carbonate precipitation. It should be noted that the modeling results show that the carbonate precipitation would rapidly increase the  $\delta^{26}\text{Mg}$  value of brine, whereas the effect of river input on reducing the Mg isotope value of brine is less significant (Fig. 10). These modeling results thus imply that additional mechanisms should be incurred to explain the rapid decrease of  $\delta^{26}\text{Mg}$  values observed in the samples (such as L-3 to L-4). We speculate that the input of a large amount of river water into the basin would decrease the salinity of brine, lowering the saturation state of the aqueous solution for the carbonate, and causing the dissolution of previously formed carbonate to release light Mg isotopes. Indeed, Hobbs and Xu (2020) suggested that repeated cycles of dissolution and reprecipitation are the key to precipitate magnesite in saline lakes, thus the dissolution of pre-existing carbonates in saline lakes could be promoted by riverine recharging events, which resulted in low  $\delta^{26}\text{Mg}$  values of the brine that could be recorded in subsequent halite precipitates formed during the next drought event.

The measured halite  $\delta^{26}\text{Mg}$  values from the XLS section indicate that the Dalangtan playa experienced humid episodes during the Mid-Pleistocene evaporite deposition (sample L-4 in Fig. 9), which is consistent with the conclusions drawn from conventional isotopic proxies (e.g.,  $\delta^{13}\text{C}$ ,  $\delta^{18}\text{O}$  and  $\delta^{37}\text{Cl}$ ). However, in contrast to the existing proxies, the halite  $\delta^{26}\text{Mg}$  value is mainly controlled by carbonate precipitation (with significant Mg isotope fractionation) and river input with limited influence on temperature and primary productivity (Kim-mig et al., 2018; Ma et al., 2019). Therefore, the Mg isotope composition of brine/halite may be used as an effective tracer of drought-wet cycles of saline lakes. Smaller fluxes of river water and low- $\delta^{26}\text{Mg}$  magnesium are imported into the basin under a dry climate, and subsequently, there would be a greater increase in  $\delta^{26}\text{Mg}$  of brine in the saline lake and the precipitated halite in response to carbonate precipitation. Correspondingly, under a humid climate, larger fluxes of fresh water and low- $\delta^{26}\text{Mg}$  magnesium are imported into the basin, which decreases the  $\delta^{26}\text{Mg}$  of the saline lake, so the brine and precipitated halite would be enriched  $^{24}\text{Mg}$  (Fig. 11). As such, the hydrological history of the Dalangtan playa during the Middle Pleistocene is reconstructed based on the halite Mg isotope data from the XLS section (Fig. 9).

## 6. Conclusions

This study presents a comprehensive isotope (C-O-Sr-Cl-Mg) and major element dataset of halite and associated carbonates in the Middle Pleistocene profile at Xiaoliangshan (XLS) of Dalangtan playa, Qaidam Basin, in northwest China. In particular, the  $\delta^{26}\text{Mg}$  values of terrestrial halite are reported for the first time.

The halite samples from the XLS section exhibit uniform  $^{87}\text{Sr}/^{86}\text{Sr}$  ratios, indicating that geochemical variabilities in the halite beds should be attributed to the hydrological fluctuation rather than changes in source materials. Compared with the major element ratios and C-O-Cl isotopic compositions, the halite  $\delta^{26}\text{Mg}$  values are more sensitive to trace the drying and recharging of the terrestrial saline lakes. The Mg isotopic composition of halite is mainly controlled by carbonate precipitation and river water input: the high  $\delta^{26}\text{Mg}$  values correspond to the precipitation of carbonate under arid climate, whereas the low  $\delta^{26}\text{Mg}$  values reflect increasing river water input in a humid climate. The remarkable variation of halite  $\delta^{26}\text{Mg}$  values in the XLS evaporite section indicates that the Dalangtan playa experienced significant fluctuations in hydrologic conditions in the Middle Pleistocene.

## Declaration of Competing Interest

The authors declare that they have no known competing financial interests or personal relationships that could have appeared to influence the work reported in this paper.

## Acknowledgements

This manuscript benefits from constructive reviews from two anonymous reviewers. We also thank Dr. Alex Dickson for editorial handling and comments. This work was supported by the Strategic Priority Research Program (B) of the Chinese Academy of Sciences (XDB26020101), the National Key R&D Program of China Project 2017YFC0602801, the National Natural Science Foundation of China (Grants No: 41622301, 41873004), and Central Public-interest Scientific Institution Basic Research Fund (Grant No: SYSCR2019-05). We thank Professor Changzhi Wu and M.N. Muthar for helping in collecting Xinjiang river samples; Yuguan Pan for the assistance of XRD analyses; Tan Bao for the assistance of halite fluid inclusion microscopic observation; Xi Liu and Ziyang Han for the help of Chlorine isotope chemistry.

## Appendix A. Supplementary data

Supplementary data to this article can be found online at <https://doi.org/10.1016/j.palaeo.2021.110804>.

## References

- Alçiçek, H., 2009. Late Miocene nonmarine sedimentation and formation of magnesites in the Acıgöl Basin, southwestern Anatolia, Turkey. *Sediment. Geol.* 219 (1), 115–135.
- Anglés, A., Li, Y., 2017. The western Qaidam Basin as a potential Martian environmental analogue: an overview. *J. Geophys. Res. Planet* 122 (5), 856–888.
- Babel, M., Schreiber, B.C., 2014. 9.17 - Geochemistry of Evaporites and Evolution of Seawater. In: Holland, H.D., Turekian, K.K. (Eds.), *Treatise on Geochemistry* (Second Edition). Elsevier, Oxford, pp. 483–560.
- Benson, L., et al., 2011. The rise and fall of Lake Bonneville between 45 and 10.5 ka. *Quat. Int.* 235, 57–69.
- Bialik, O.M., et al., 2018. Mg isotope response to dolomitization in hinterland-attached carbonate platforms: outlook of  $\delta^{26}\text{Mg}$  as a tracer of basin restriction and seawater Mg/Ca ratio. *Geochim. Cosmochim. Acta* 235, 189–207.
- Chen, X.-Y., et al., 2020. Experimental constraints on magnesium isotope fractionation during abiogenic calcite precipitation at room temperature. *Geochim. Cosmochim. Acta* 281, 102–117.
- Cheng, R.-L., He, H., Michalski, J.R., Li, Y.-L., 2021. A new type of polygonal terrain formed by sulfate weathering in arid regions. *Geomorphology* 383, 107695.
- De Muynck, D., Huelga-Suarez, G., Van Heghe, L., Degryse, P., Vanhaecke, F., 2009. Systematic evaluation of a strontium-specific extraction chromatographic resin for obtaining a purified Sr fraction with quantitative recovery from complex and Ca-rich matrices. *J. Anal. At. Spectrom.* 24 (11), 1498–1510.
- Deocampo, D.M., Jones, B.F., 2014. 7.13 - Geochemistry of Saline Lakes. In: Holland, H. D., Turekian, K.K. (Eds.), *Treatise on Geochemistry* (Second Edition). Elsevier, Oxford, pp. 437–469.
- Du, Y., et al., 2019. Evaluation of boron isotopes in halite as an indicator of the salinity of Qarhan paleolake water in the eastern Qaidam Basin, western China. *Geosci. Front.* 10 (1), 253–262.
- Eastoe, C.J., Peryt, T., 1999. Stable chlorine isotope evidence for non-marine chloride in Badenian evaporites, Carpathian mountain region. *Terra Nova* 11, 118–123.
- Eggenkamp, H.G.M., Kreulen, R., Koster Van Groos, A.F., 1995. Chlorine stable isotope fractionation in evaporites. *Geochim. Cosmochim. Acta* 59, 5169–5175.
- Eugster, H.P., 1980. Geochemistry of evaporitic lacustrine deposits. *Annu. Rev. Earth Planet. Sci.* 8 (1), 35–63.
- Fan, Q., et al., 2018. Sr isotope and major ion compositional evidence for formation of Qarhan Salt Lake, western China. *Chem. Geol.* 497, 128–145.
- Feng, C., et al., 2018. Tracking physicochemical conditions of evaporite deposition by stable magnesium isotopes: a case study of Late Permian Langbeinites. *Geochim. Cosmochim. Acta* 19 (8), 2615–2630.
- Flecker, R., de Villiers, S., Ellam, R.M., 2002. Modelling the effect of evaporation on the salinity- $87\text{Sr}/86\text{Sr}$  relationship in modern and ancient marginal-marine systems: the Mediterranean Messinian Salinity Crisis. *Earth Planet. Sci. Lett.* 203 (1), 221–233.
- Guo, P., et al., 2018. Palaeohydrological evolution of the late Cenozoic saline lake in the Qaidam Basin, NE Tibetan Plateau: Tectonic vs. climatic control. *Glob. Planet. Chang.* 165, 44–61.
- Hay, W., et al., 2006. Evaporites and the salinity of the ocean during the phanerozoic: implications for climate, ocean circulation and life. *Palaeogeogr. Palaeoclimatol. Palaeoecol.* 240, 3–46.
- Hobbs, F.W.C., Xu, H., 2020. Magnesite formation through temperature and pH cycling as a proxy for lagoon and playa paleoenvironments. *Geochim. Cosmochim. Acta* 269, 101–116.
- Horita, J., 2014. Oxygen and carbon isotope fractionation in the system dolomite-water-CO<sub>2</sub> to elevated temperatures. *Geochim. Cosmochim. Acta* 129, 111–124.
- Hu, Z., et al., 2017. Resetting of Mg isotopes between calcite and dolomite during burial metamorphism: outlook of Mg isotopes as geothermometer and seawater proxy. *Geochim. Cosmochim. Acta* 208, 24–40.
- Huang, Q., Ku, T.-L., Phillips, F.M., 1993. Evolutionary characteristics of lakes and palaeoclimatic undulation in the Qaidam Basin, China. *Chin. J. Oceanol. Limnol.* 11 (01), 34–45.
- Immenhauser, A., et al., 2010. Magnesium-isotope fractionation during low-Mg calcite precipitation in a limestone cave – Field study and experiments. *Geochim. Cosmochim. Acta* 74 (15), 4346–4364.
- Jin, Z.D., Wang, S., Zhang, F., Shi, Y., 2010. Weathering, Sr fluxes, and controls on water chemistry in the Lake Qinghai catchment, NE Tibetan Plateau. *Earth Surf. Process. Landf.* 35, 1057–1070.
- Johnson, C.M., Beard, B.L., Albarède, F., 2004. Geochemistry of non-traditional stable isotopes. *Rev. Mineral. Geochem.* 55, 1–24.
- Kimmig, S.R., Holmden, C., Bélanger, N., 2018. Biogeochemical cycling of Mg and its isotopes in a sugar maple forest in Québec. *Geochim. Cosmochim. Acta* 230, 60–82.
- Kong, W.G., Zheng, M.P., Kong, F.J., Chen, W.X., 2014. Sulfate-bearing deposits at Dalangtan Playa and their implication for the formation and preservation of martian salts. *Am. Mineral.* 99 (2–3), 283–290.
- Kong, F., et al., 2018. Dalangtan Saline Playa in a hyperarid region on Tibet Plateau: I. Evolution and environments. *Astrobiology* 18 (10), 1243–1253.
- Li, H.-C., Ku, T., 1997.  $\delta^{13}\text{C}$ - $\delta^{18}\text{O}$  covariance as a paleohydrological indicator for closed-basin lakes. *Palaeogeogr. Palaeoclimatol. Palaeoecol.* 133, 69–80.
- Li, W., Beard, B.L., Johnson, C.M., 2011. Exchange and fractionation of Mg isotopes between epsomite and saturated MgSO<sub>4</sub> solution. *Geochim. Cosmochim. Acta* 75 (7), 1814–1828.
- Li, W., Chakraborty, S., Beard, B.L., Romanek, C.S., Johnson, C.M., 2012a. Magnesium isotope fractionation during precipitation of inorganic calcite under laboratory conditions. *Earth Planet. Sci. Lett.* 333–334, 304–316.
- Li, X., Liu, W., Xu, L., 2012b. Carbon isotopes in surface-sediment carbonates of modern Lake Qinghai (Qinghai-Tibet Plateau): Implications for lake evolution in arid areas. *Chem. Geol.* 88–96 s 300–301.
- Li, W., Beard, B.L., Li, C., Xu, H., Johnson, C.M., 2015. Experimental calibration of Mg isotope fractionation between dolomite and aqueous solution and its geological implications. *Geochim. Cosmochim. Acta* 157, 164–181.
- Li, W., et al., 2019. Effects of early diagenesis on Mg isotopes in dolomite: the roles of Mn (IV)-reduction and recrystallization. *Geochim. Cosmochim. Acta* 250, 1–17.
- Li, J., Zhu, L., Li, M., Wang, J., Ma, Q., 2020. Origin of modern dolomite in surface lake sediments on the central and western Tibetan Plateau. *Quat. Int.* 544.
- Liu, W., Li, X., An, Z., Xu, L., 2009. Evaluation of oxygen isotopes in carbonate as an indicator of lake evolution in arid areas: the modern Qinghai Lake, Qinghai-Tibet Plateau. *Chem. Geol.* 268, 126–136.
- Lowenstein, T.K., Li, J., Brown, C., Roberts, S.M., Yang, W., 1999. Paleoclimate record from Death Valley salt core. *Geology* 27 (1), 3–6.
- Lu, F., Meyers, W., 2003. Sr, S, and SO<sub>4</sub> isotopes and the depositional environments of the Upper Miocene evaporites, Spain. *J. Sediment. Res.* 73 (3), 444–450.
- Luo, C., et al., 2012. Stable isotope fractionation of chlorine during evaporation of brine from a saline lake. *Chin. Sci. Bull.* 57 (15), 1833–1843.
- Luo, C., et al., 2016. Chlorine isotopes in sediments of the Qarhan Playa of China and their paleoclimatic significance. *Geochim. Cosmochim. Acta* 176 (1), 149–156.
- Ma, N.N., et al., 2011. Forming age of surface mirabilite in Dalangtan, Qaidam Basin and its environmental significance. *Acta Geol. Sin.* (in Chinese with English abstract) 85, 433–444.
- Ma, L., et al., 2019. Tracing changes in monsoonal precipitation using Mg isotopes in Chinese loess deposits. *Geochim. Cosmochim. Acta* 259, 1–16.
- Mavromatis, V., Gautier, Q., Bosc, O., Schott, J., 2013. Kinetics of Mg partition and Mg stable isotope fractionation during its incorporation in calcite. *Geochim. Cosmochim. Acta* 114, 188–203.
- McCaffrey, M.A., Lazar, B., Holland, H.D., 1987. The evaporation path of seawater and the coprecipitation of Br<sup>-</sup> and K<sup>+</sup> with halite. *J. Sediment. Petrol.* 57 (5), 928–938.
- Melezhik, V.A., Fallick, A.E., Medvedev, P.V., Makarikhin, V.V., 2001. Palaeoproterozoic magnesite: lithological and isotopic evidence for playa/sabkha environments. *Sedimentology* 48 (2), 379–397.
- Moretto, R., 1988. Observations on the incorporation of trace elements in halite of Oligocene salt beds, Bourg-en-Bresse Basin, France. *Geochim. Cosmochim. Acta* 52 (12), 2809–2814.
- Newell, D., Jensen, J., Frantz, C., Vanden Berg, M., 2017. Great Salt Lake (Utah) microbialite  $\delta^{13}\text{C}$ ,  $\delta^{18}\text{O}$ , and  $\delta^{15}\text{N}$  record fluctuations in Lake biogeochemistry since the Late Pleistocene. *Geochim. Cosmochim. Acta* 18 (10), 3631–3645.
- Pilson, M.E.Q., 2012. *An Introduction to the Chemistry of the Sea*, Second ed. Cambridge University Press, Cambridge.
- Pogge von Strandmann, P.A.E., Olsson, J., Luu, T.-H., Gislason, S.R., Burton, K.W., 2019. Using Mg isotopes to estimate natural calcite compositions and precipitation rates during the 2010 Eyjafjallajökull eruption. *Front. Earth Sci.* 7 (6).
- Roberts, S.M., Spencer, R.J., 1995. Paleotemperatures preserved in fluid inclusions in halite. *Geochim. Cosmochim. Acta* 59 (19), 3929–3942.
- Shalev, N., et al., 2018a. Mg isotope interlaboratory comparison of reference materials from earth-surface low-temperature environments. *Geostand. Geoanal. Res.* 42 (2), 205–221.
- Shalev, N., Lazar, B., Köbberich, M., Halicz, L., Gavrieli, I., 2018b. The chemical evolution of brine and Mg-K-salts along the course of extreme evaporation of seawater – An experimental study. *Geochim. Cosmochim. Acta* 241, 164–179.
- Shalev, N., Bontognali, T.R.R., Vance, D., 2020. Sabkha dolomite as an archive for the magnesium isotope composition of seawater. *Geology* 49 (3), 253–257.
- Shalev, N., Lazar, B., Halicz, L., Gavrieli, I., 2021. The Mg isotope signature of marine Mg-evaporites. *Geochim. Cosmochim. Acta* 301, 30–47.
- Sobron, P., et al., 2018. Dalangtan Saline Playa in a hyperarid region of Tibet Plateau: III. Correlated multiscale surface mineralogy and geochemistry survey. *Astrobiology* 18 (10), 1277–1304.

- Son, S., Li, W., Lee, J.-Y., Kwon, K.D., 2020. On the coordination of Mg<sup>2+</sup> in aragonite: Ab-initio absorption spectroscopy and isotope fractionation study. *Geochim. Cosmochim. Acta* 286, 324–335.
- Song, B., et al., 2020. Miocene 87Sr/86Sr ratios of ostracods in the northern Qaidam Basin, NE Tibetan Plateau, and links with regional provenance, weathering and eolian input. *Palaeogeogr. Palaeoclimatol. Palaeoecol.* 552, 109775.
- Stiller, M.S., Shasha, J., 1985. Extreme carbon isotope enrichments in evaporating brines. *Nature* 316, 434–435.
- Sun, S., et al., 2019. Bromine content and Br/Cl molar ratio of halite in a core from Laos: implications for origin and environmental changes. *Carbonates Evaporites* 34, 1107–1115.
- Talbot, M.R., 1990. A review of the palaeohydrological interpretation of carbon and oxygen ratios in primary lacustrine carbonates. *Chem. Geol. Isotope Geosci. Sect.* 80, 261–279.
- Tan, H., Ma, H., Xiao, Y., Wei, H., Man, W., 2005. Characteristics of chlorine isotope distribution and analysis on sylvinitic deposit formation based on ancient salt rock in the western Tarim Basin. *Sci. China Ser. D* 48 (11), 1913–1920.
- Tan, H., Ma, H., Wei, H., Xu, J., Li, T., 2006. Chlorine, sulfur and oxygen isotopic constraints on ancient evaporite deposit in the Western Tarim Basin, China. *Geochem. J.* 40, 569–577.
- Teng, F.-Z., 2017. Magnesium isotope geochemistry. *Rev. Mineral. Geochem.* 82 (1), 219–287.
- Tipper, E., et al., 2006. The magnesium isotope budget of the modern ocean: constraints from riverine magnesium isotope ratios. *Earth Planet. Sci. Lett.* 250 (1–2), 241–253.
- Ullman, W., Collerson, K., 1994. The Sr-isotope record of late Quaternary hydrologic changes around Lake Frome, South Australia. *Aust. J. Earth Sci.* 41, 37–45.
- Wang, B., 2006. *The Asian Monsoon*. Praxis/Springer, Berlin, Heidelberg.
- Wang, A., Zheng, M., Kong, F., Sobron, P., Mayer, D., 2010. Saline Playas on Qinghai-Tibet Plateau as Mars Analog for the Formation-Preservation of Hydrous Salts and Biosignatures (AGU Fall Meeting Abstracts).
- Wang, Z., et al., 2013. Experimental calibration of Mg isotope fractionation between aragonite and seawater. *Geochim. Cosmochim. Acta* 102, 113–123.
- Wang, A., Sobron, P., Kong, F., Zheng, M., Zhao, Y.S., 2018. Dalangtan Saline Playa in a hyperarid region on Tibet Plateau: II. Preservation of salts with high hydration degrees in subsurface. *Astrobiology* 18 (10), 1254–1276.
- Wang, W., Zhou, C., Liu, Y., Wu, Z., Huang, F., 2019. Equilibrium Mg isotope fractionation among aqueous Mg<sup>2+</sup>, carbonates, brucite and lizardite: insights from first-principles molecular dynamics simulations. *Geochim. Cosmochim. Acta* 250, 117–129.
- Wang, W.-Q., et al., 2021. Revisiting the Permian seawater 87Sr/86Sr record: new perspectives from brachiopod proxy data and stochastic oceanic box models. *Earth Sci. Rev.* 218, 103679.
- Warren, J., 2010. Evaporites through time: Tectonic, climatic and eustatic controls in marine and nonmarine deposits. *Earth Sci. Rev.* 98, 217–268.
- Warren, J.K., 2016. *Evaporites a Geological Compendium (Second Edition)*. Springer.
- Wei, H.-Z., et al., 2012. Precise determination of the absolute isotopic abundance ratio and the atomic weight of chlorine in three international reference materials by the positive thermal ionization mass spectrometer-Cs<sub>2</sub>Cl<sup>+</sup>–graphite method. *Anal. Chem.* 84 (23), 10350–10358.
- Wu, W., 2016. Hydrochemistry of inland rivers in the north Tibetan Plateau: constraints and weathering rate estimation. *Sci. Total Environ.* 541, 468–482.
- Wu, W., Xu, S., Yang, J., Yin, H., Tao, X., 2009. Sr fluxes and isotopic compositions in the headwaters of the Yangtze River, Tongtian River and Jinsha River originating from the Qinghai–Tibet Plateau. *Chem. Geol.* 260 (1), 63–72.
- Xia, J., Ito, E., Engstrom, D.R., 1997. Geochemistry of ostracode calcite: part 1. An experimental determination of oxygen isotope fractionation. *Geochim. Cosmochim. Acta* 61, 377–382.
- Xia, Z., et al., 2020. Extracting Mg isotope signatures of ancient seawater from marine halite: a reconnaissance. *Chem. Geol.* 552, 119768.
- Xiao, Y.K., et al., 2002. A secondary isotopic reference material of chlorine from selected seawater. *Chem. Geol.* 182, 655–661.
- Xiao, L., et al., 2017. A new terrestrial analogue site for Mars research: the Qaidam Basin, Tibetan Plateau (NW China). *Earth Sci. Rev.* 164, 84–101.
- Yadav, D., 1997. Oxygen isotope study of evaporating brines in Sambhar Lake, Rajasthan (India). *Chem. Geol.* 138, 109–118.
- Zhang, H., et al., 2018. Fractionation of Mg isotopes by clay formation and calcite precipitation in groundwater with long residence times in a sandstone aquifer, Ordos Basin, China. *Geochim. Cosmochim. Acta* 237, 261–274.
- Zhang, P., et al., 2021. Magnesium isotope fractionation during alkaline brine evaporation and implications for Precambrian seawater chemistry. *Chem. Geol.* 585. <https://doi.org/10.1016/j.chemgeo.2021.120565>.
- Zhao, Y., et al., 2020. Isotope evidence for multiple sources of B and Cl in Middle Miocene (Badenian) evaporites, Carpathian Mountains. *Appl. Geochem.* 104819.
- Zheng, M., 1997. *An Introduction to Saline Lakes on the Qinghai–Tibet Plateau*. Boston.
- Zheng, M., Tang, J., Liu, J., Zhang, F., 1993. Chinese saline lakes. *Hydrobiologia* 267 (1), 23–36.
- Zheng, M., Wang, A., Kong, F., Ma, N., 2009. Saline Lakes on Qinghai-Tibet Plateau and Salts on Mars, In 40th Lunar and Planetary Science Conference Abstracts, Houston.